LA-UR- 10-01472

Approved for public release; distribution is unlimited.

Title:	Influence of Hot Spot Features on the Initiation Characteristics of Heterogeneous Nitromethane
Author(s):	D. M. Dattelbaum, S. A. Sheffield, D. B. Stahl, A. M. Dattelbaum, W. Trott, R. Engelke
Intended for:	International Detonation Symposium, conference proceedings

Los Alamos
NATIONAL LABORATORY
EST. 1943

Form 836 (7/06)

Influence of Hot Spot Features on the Initiation Characteristics of Heterogeneous Nitromethane

Dana M. Dattelbaum*, Stephen A. Sheffield*, David B. Stahl*, Andrew M. Dattelbaum*, Wayne Trott, R. Engelke*

*Shock and Detonation Physics
Los Alamos National Laboratory, Los Alamos, NM 87545

Sandia National Laboratory, Albuquerque, NM 87185

Abstract. To gain insights into the critical hot spot features influencing energetic materials initiation characteristics, well-defined micron-scale particles have been intentionally introduced into the homogeneous explosive nitromethane (NM). Two types of potential hot spot origins have been examined -- shock impedance mismatches using solid silica beads, and porosity using hollow microballoons – as well as their sizes and inter-particle separations. Here, we present the results of several series of gas gun-driven plate impact experiments on NM/particle mixtures with well-controlled shock inputs. Detailed insights into the nature of the reactive flow during the build-up to detonation have been obtained from the response of in-situ electromagnetic gauges, and the data have been used to establish Pop-plots (run-distance-to-detonation vs. shock input pressure) for the mixtures. Comparisons of sensitization effects and energy release characteristics relative to the initial shock front between the solid and hollow beads are presented.

Introduction

Shock initiation in heterogeneous explosives is widely acknowledged to be derived from the formation of "hot spots," or highly localized regions of high temperature and pressure, from which chemistry originates.[1-20] Hot spot concepts, as they pertain to explosives initiation, date back over 50 years.[1-3] Bowden and Yoffe estimated the critical size ~0.1-10 micron, temperature >700K, and temporal duration of 10^{-5}-10^{-3} s of hot spots.[1] A number of experimental studies have since aimed to unravel the links between microstructural details, hot spot formation and growth, and bulk explosives response. For example, investigations linking explosive grain size to either the critical diameter or run-distance-to-detonation have been performed for formulations containing RDX, PETN, and TNT.[8-11] Further, porosity has been investigated for its role in hot spot formation, through the study of pressed explosives at varying initial densities and by the introduction of glass microballoons into liquid, slurry, and solid explosives.[12-15] From a theoretical standpoint, hot spot concepts form the basis of the ignition and growth model[16], where the model treats separate hot spot ignition and growth phases, in practice calibrated to experimental shock initiation data.

Here, we report the results of an experimental study aimed at determining critical features of hot spots and their relation to shock initiation mechanisms and thresholds. We have chosen gelled nitromethane as a model system that offers an ability to vary features of the microstructure in

the mixture while maintaining the basic explosive provides a system that is useful for interrogating hot spot type, size, shape, and number density. Both solid and hollow glass spheres, of relevant sizes in the micron-range, have been intentionally introduced into the otherwise-homogeneous liquid explosive nitromethane (NM). Here, we present results of shock initiation experiments focused on hot spot type, e.g. probing the relative effectiveness of shock impedance mismatches and porosity as two types of hot spot seeds, number density and size. In addition to measurements of the run-distance-to-detonation (Pop-plot)[7] as a function of shock input pressures, the application of embedded electromagnetic gauges allows for *in-situ* measurements of the wave profiles, giving insights into the nature of the reactive flow and build-up to detonation as the hot spot details are varied.

Background

Homogeneous explosives, such as neat liquid nitromethane, exhibit fundamentally different shock initiation behaviors compared with solid, multi-phase explosives. The initiation "mechanism" for liquid explosives is marked by shock heating of the material, giving rise to a thermal explosion that occurs behind the incident shock front after a characteristic induction time.[26-28] Following the thermal explosion, growth of a reactive wave behind the front is observed, building up over measureable time and distance until it reaches a steady condition or overtakes the initial shock.[28] The steady wave is referred to as a superdetonation, observed to travel at high velocities exceeding 10 km/s (Lagrangian) because they travel in a shock pre-compressed material. Once a reactive wave overtakes the front, an overdriven detonation is observed which settles down to a steady detonation with distance (x) or time (t) (shown in Figure 1 top). "Heterogeneous" or multi-phase explosives, such as plastic bonded explosives, by contrast, typically show reactive growth in or near (in time/distance) the shock front, with gradual, continuous reactive growth eventually leading to steady detonation, Fig. 1 bottom. Many heterogeneous explosives have been shown to exhibit shock initiation behavior that is reminiscent of both mechanisms, with the reactive growth lagging, but steadily building behind the front.[35]

Neat NM is one of the most well-characterized liquid explosives in terms of its equation of state (EOS), shock initiation and detonation properties.[4-6,24-33] NM has a steady detonation velocity of 6.23 mm/μs, estimated Chapman-Jouguet (CJ) pressure P_{CJ} = 12.5 GPa, and failure diameter of 16.2 mm in pyrex glass.[4] Its chemical reaction zone is characterized by an estimated von Neumann (vN) spike particle velocity of ~2.7 mm/μs, and CJ state at 1.8 mm/μs, with fast (~10 ns) and slow (~100 ns) components behind the front.[24] The Pop-plot for neat NM has been well-established by numerous sources, and representative data are shown by the open symbols in Fig. 2.[7,28-31]

The detonation properties of NM have been previously shown to be susceptible to both chemical and physical sensitization as shown by either reduction in critical (failure) diameters, or lowering of shock initiation thresholds.[4-6,17-19]

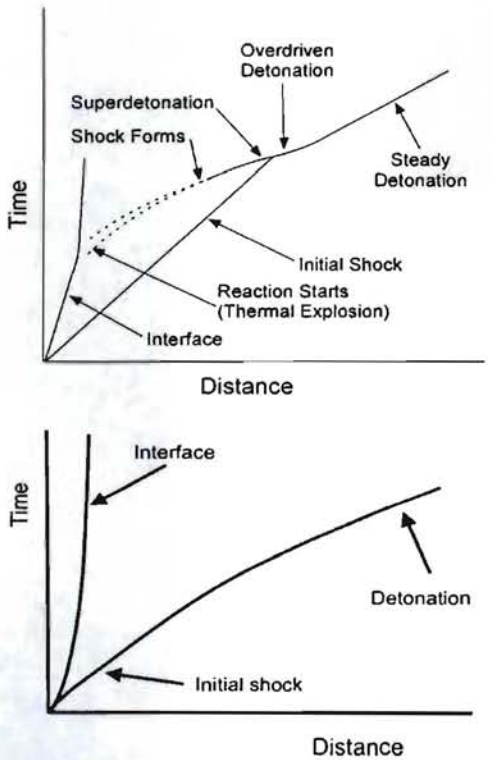

Figure 1. Time-distance (t-x) diagrams illustrating the difference in shock initiation mechanisms

between (top) a homogeneous liquid explosive, and (bottom) a heterogeneous explosive.

Engelke has shown that the addition of rough (uncontrolled particle morphologies, 5-75 μm diameters) silica at 6 wt% to NM, gelled with guar gum, results in a dramatic reduction in the critical diameter compared to neat NM.[4] Engelke further performed a series of failure diameter experiments, varying the number density and diameter of controlled size silica beads in gelled NM. He found that reductions in the critical diameter were most profound for small (1-4 μm) silica beads, and that there is a correlation between the reduction in critical diameter and mean interparticle separation.[5] Similarly, Bouton *et al.* has suggested that both the critical diameter and run-distance-to-detonation at fixed input shock pressure can be correlated with the specific surface area of either the explosive grains, or inert additives that are suspected to give rise to hot spots.[19]

Recently, we have shown that the initiation behavior of NM:6 wt% rough silica solutions is also quite different than neat NM. The shock input pressure is substantially lowered for the same time-to-detonation compared with neat NM, Fig. 2.[28-33] Examination of the shock and reactive wave evolution in the shock-to-detonation transition reveals that the mechanism of the build-up to detonation is consistent with heterogeneous explosives, described above. Here, we build on these preliminary results by controlling the particle sizes, types (solid or hollow), and volumetric loadings of potential hot spot "seeds."

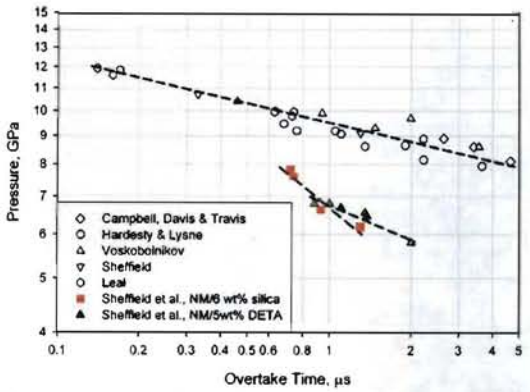

Figure 2. Pop-plots for neat NM from multiple sources (see text) and NM/rough silica at 6 wt%. For comparison, the Pop-plot data for 95% NM/5 wt% DETA (diethylene triamine) is also shown.[6]

Experimental

Nitromethane (NM, CH_3NO_2) was purchased from Sigma-Aldrich (99+%) and used without further purification, with a freshly-opened sample used for each experiment. Guar gum (General Mills 512 Guar, a cyanoethylether of a galactomannan gum), was the same as that used by Engelke, and was added slowly to gel the solutions at 1.75 wt%.[4,5] Solid silica particles with 1-4 and 40 μm diameters were obtained from Particle Information Services. Hollow glass bubbles (K46) were obtained from 3M, Inc., and were sieved prior to use to a size range of 38-45 μm. Particle sizes in both cases were confirmed using both optical and scanning electron microscopies. Interparticle spacings (L) were estimated from volume occupied by single particles $L \approx V^{1/3}$, where $V = \frac{4}{3}\pi r^3 \rho_p / (w_p \rho_s)$. r is the mean particle radius. ρ_p and ρ_s are the densities of the particles and NM solutions, respectively. w_p is the weight percentage of the particles in the NM solutions.[5]

Samples for plate-impact experiments were prepared by weighing out appropriate quantities of NM, Guar, and particles to prepare mixtures gelled with 1.75 wt% Guar. Solid particles were incorporated into NM/Guar solutions at a constant 6 wt% (ρ_s = 1.15 g/cm^3, 92.25 wt% NM, 1.75 wt% Guar, and 6 wt% silica). Hollow microballoons were added at 1.2 and 0.36 wt% to NM/1.85 wt% Guar solutions (ρ_s = 1.06-1.07 g/cm^3). The particles were added to the NM in a high-walled beaker, followed by slow addition of Guar with continuous stirring to gel the mixture. The resulting white, viscous mixture was then pipetted into a LANL-designed liquid target cell.[6,28] A photograph of a partially assembled target cell is shown in Figure 3.

Plate-impact experiments were performed using the LANL 50 mm-bore two-stage light gas gun described previously.[23] Kel-F 81 (polychlorotrifluoroethylene) impactors saboted in

Lexan projectiles were launched at velocities up to ~2.9 km/s at instrumented targets containing the NM mixtures.

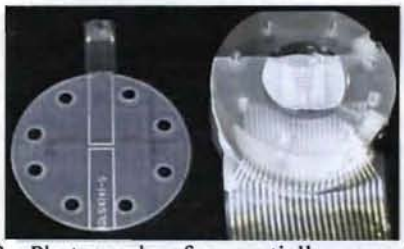

Figure 3. Photograph of a partially assembled liquid target cell with the top off, showing the embedded electromagnetic gauge at a 30° angle.

Embedded electromagnetic gauges, described previously,[21-23] provided *in-situ* particle velocity profiles at ten Lagrangian positions, allowing for determination of both the initial, unreacted shocked state (Hugoniot locus) and run-distance (or time)-to-detonation. In one experiment, 2S-437, the gauge membrane was inserted at a 10° angle (vs. the usual 30°) to measure the shock-to-detonation transition at a short run distance. The input shock pressure was determined by the measurement of the initial shock and particle velocities and application of the Rankine-Hugoniot conservation equations or by impedance matching methods using the measured initial particle velocity and Kel-F 81 Hugoniot-based equation of state. The time to detonation was determined as the time from the initial shock input into the NM mixture to the observation of a leading detonation wave at the embedded gauge elements (or Lagrangian positions).

Measurements of the chemical reaction zone for neat NM and NM/1.2 wt% glass microballoons were performed by using gas gun-driven plate impact to initiate samples contained in 25 mm diameter pyrex cylinders, nominally 6 diameters long to ensure steady detonation, as described previously.[24]

Results

Shock initiation experiments have been performed on nitromethane/particle solutions containing both solid silica beads and hollow glass microballoons. The results from experiments on the two different types of hot spots (impedance mismatches vs. void collapse) and a comparison between them are presented below.

Solid particle loadings

Over a dozen gas gun-driven shock initiation experiments have been performed on gelled nitromethane samples containing size-selected solid silica beads with diameters of 1-4 μm or 40 μm at 6 wt%. The particles are the same as used previously by Engelke.[5] In the 6 wt% 40 μm bead solutions, the inter-bead distance is ~106 μm. Keeping the weight percentage constant increases the volumetric loading in the small (1-4 μm) bead NM/particle solutions, giving an inter-bead distance of only ~ 6 μm. The results of two series of experiments are summarized in Table 1, and have been presented, in part, previously.[36] The Pop-plot data points for the two mixtures are overlaid with a line representing neat NM in Figure 4. Shock initiation in neat NM occurs at initial shock pressures below the CJ detonation pressure, but still at significantly higher input pressures than conventional plastic-bonded explosives such as PBX 9501.[35] Generally, the addition of solid silica beads at 6 wt% to NM has a sensitizing effect, lowering the initiation thresholds by as much as 2-3 GPa, depending on the mixture, shock input pressure and run distance regime.

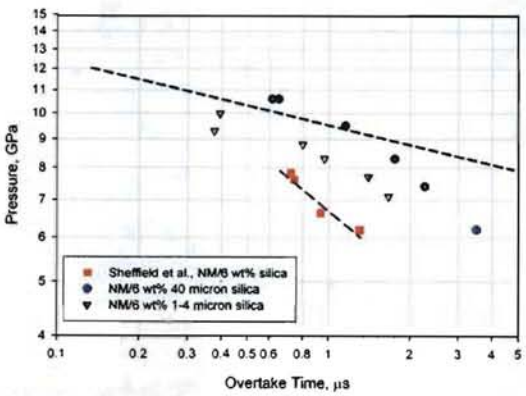

Figure 4. Pop-plots for NM/6 wt% silica with 1-4 and 40 μm silica beads, compared with neat NM and NM/6 wt% rough silica.

The solutions containing larger beads, spaced by ~ 2.5 diameters, show unprecedented shock

initiation behavior. Examination of the Pop-plot data in Fig. 4 shows a greater slope in this plane at lower input pressures, and a "bending over" of the data to parallel the neat NM data at high input pressures. To our knowledge, this is the first time this non-linear Pop-plot behavior has been demonstrated. Further, the evolution of the Pop-plot as a function of shock strength is coincident with changes in the nature of the build-up to detonation. Figures 5 and 6 show the in-situ wave profiles recorded for shots 2S-358 and 2S-317, respectively. As the shock input pressure is lowered, greater reactive growth is observed near the shock front, as evidenced by an increase in the particle velocity directly behind the shock front. At low pressures (<6 GPa, 2S-312 not shown), reactive growth closely behind the shock front was observed, but the material did not turn-over to detonation within the time/distance of the gauge elements and 1-dimensionality of the experiment. This behavior is suggestive of hot spot-driven reactive growth. At intermediate shock input pressures (7-8 GPa), both growth near the front, and the development of a reactive wave behind he front are observed, Fig. 5.

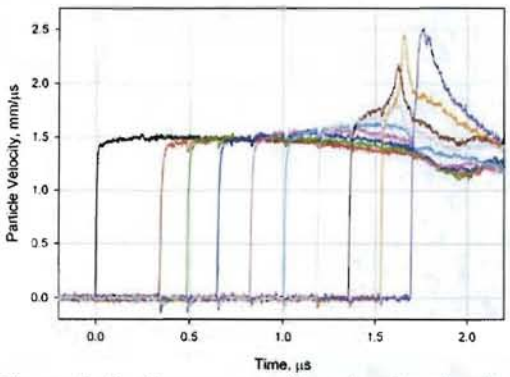

Figure 5. *In-situ* wave profiles showing the shock-to-detonation transition for shot 2S-358, 92.25/6.0/1.75 NM/40μm silica/Guar, with an initial shock input pressure of 7.8 GPa.

Greater inspection of the wave profiles in Fig. 5 reveals a drop in particle velocity in the gauge records associated with the Lagrangian positions ahead of the reactive wave, coincident with the appearance of the trailing wave, indicative of a thermal explosion, similar to that observed in homogenous liquid explosives. This behavior is recorded in Table I as "mixed mechanism." Here, there appears to be two mechanisms at play, pointing to ineffective hot spot coordination on the timescale of bulk shock heating-driven thermal explosion.

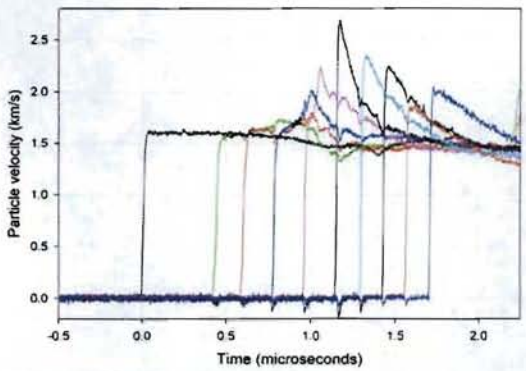

Figure 6. *In-situ* wave profiles showing the shock-to-detonation transition for shot 2S-317, 92.25/6.0/1.75 NM/40μm silica/Guar, with an initial shock input pressure of 9.5 GPa.

Finally, at high shock input pressures (>9.5 GPa), the initiation behavior is nearly indistinguishable from homogeneous NM, with clear evidence of the classic features of homogenous initiation including overdriven detonation following overtake, Fig. 6. To our knowledge, this is one of the few (if any) direct observations of a homogeneous initiation mechanism in a heterogeneous explosive formulation. At these shock pressures, hot spot coordination is secondary to thermal-driven chemistry.

By contrast, the NM solutions containing 6 wt% small (1-4 μm) beads show consistent heterogeneous initiation behavior across the range of input shock pressures investigated. Fig. 7 shows the wave profiles measured for shot 2S-361 with an initial shock input pressure of 8.5 GPa. Here, and across the series of shots, the reactive flow associated with the build-up to detonation is marked by an increase in particle velocity near, but slightly delayed behind the front, consistent with the initiation behavior of PBXs, and a hallmark of effective hot spot-driven reactive growth. Here, the volumetric concentration of hot spots is

Table 1. Summary of shock initiation experiments on heterogeneous NM with controlled silica particle diameters. P_{in} is the input shock pressure in GPa, t is the shock-to-detonation run time in microseconds.

Shot #	Projectile velocity (km/s)	Particle loading/size	P_{in} (GPa)	Time-to-detonation (μs)	Comments
2S-312	2.045	6 wt% 40 μm solid beads	6.2	>3.5	Did not turn over
2S-314	2.308	6 wt% 40 μm silica	7.4	2.26	Mixed mechanism
2S-317	2.721	6 wt% 40 μm silica	9.5	1.15	Homogeneous-like
2S-356	2.904	6 wt% 40 μm silica	10.6	0.65	Homogeneous-like
2S-357	2.909	6 wt% 40 μm silica	10.6	0.62	Homogeneous-like[6]
2S-358	2.485	6 wt% 40 μm silica	8.3	1.75	Mixed mechanism
2S-319	2.669	6 wt% 1-4 μm silica	9.3	~0.38	Early turn-over
2S-359	2.235	6 wt% 1-4 μm silica	7.0	1.66	Growth in and behind front
2S-361	2.468	6 wt% 1-4 μm silica	8.2	0.96	Growth in and behind front
2S-397	2.350	6 wt% 1-4 μm silica	7.7	1.44	Growth in and behind front
2S-398	2.570	6 wt% 1-4 μm silica	8.8	0.71	Growth in and behind front
2S-437	2.801	6 wt% 1-4 μm silica	9.9	0.39	Growth in and behind front
2S-438	2.245	1.2 wt% 40 μm hollow balloons	7.2	1.08	Heterogeneous
2S-441	2.520	1.2 wt% 40 μm hollow balloons	8.2	0.88	Heterogeneous
2S-442	2.520	1.2 wt% 40 μm hollow balloons	8.1	1.51	Mixed mechanism
2S-444	2.797	1.2 wt% 40 μm hollow balloons	9.2	0.94	Mixed mechanism

expected to be much greater, since the beads are spaced only ~ 6 μm apart. The Pop-plot for this mixture is lowered (sensitized) compared with neat NM, and there may be evidence of a slope change at lower shock input pressures (< 8 GPa). This mixture indicates that coordination between hot spots derived from shock impedance mismatches is effective on this length scale. Once detonating, it appears that the chemical reaction zone may be altered by the hot spot-driven burn as well. There is a clear discontinuity (near u_p ~ 1.8 mm/μs) in the particle velocity wave profile over its decay from the peak.

The insights gained from the shock initiation experiments on the solid bead solutions appear qualitatively consistent with Engelke's critical diameter work.[4-5] Here, we see that, *at high input shock pressures*, the presence of large silica beads appear to have little effect on the run distance to detonation or reactive flow characteristics. Though run-distance-to-detonation is not directly correlated to critical diameter, Engelke observed no effect on the critical diameter for similar solutions.[5]

Further, by increasing the number density and thus decreasing the distance between the particles, the initiation behavior is consistently hot spot-driven, and sensitized compared with neat NM. Engelke also observed a clear decrease in the critical diameter in solutions that correlated linear with a decrease in interparticle spacings in this range. Non-reactive simulations of the hydrodynamic flow in nitromethane with 20 μm silica beads shocked to 10 GPa suggest that the mechanism for hot spot formation is a combination of adjacent wave collisions occurring between the beads, as well as Mach reflections at the bead-NM interface.[34] Shock reflections normal to the NM-bead interface were not found to appreciably raise the temperature.

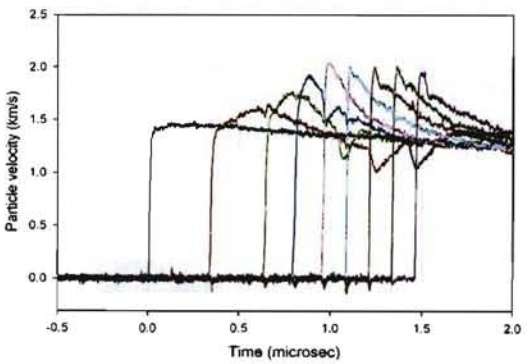

Figure 7. *In-situ* wave profiles showing the shock-to-detonation transition for shot 2S-361, 92.25/6.0/1.75 NM/1-4 μm silica/Guar, with an initial shock input pressure of 8.5 GPa.

Finally, the detonation velocity for the NM/silica with 6 wt% 1-4 μm beads could be estimated from shot 2S-319. In this experiment, the turnover to detonation occurred near the impact interface, and the detonation appeared to be nearly-steady as recorded by the gauges located farther from the interface. The detonation velocity was found to be 6.152 ± 0.017 km/s from the response of one of the shock trackers, which compares well with D_e = 6.167 ± 0.002 km/s reported for NM:silica by Engelke.[4]

Hollow glass microballoons

A smaller series of experiments have been performed on NM mixtures containing hollow glass microballoons as a second type of hot spot "seed" – e.g. porosity or void collapse. Glass microballoons (ρ_0= 0.46 g/cm^3), sieved to isolate nominally 38-45 μm diameter particles, were incorporated into gelled NM at two different volumetric loadings.

The first two experiments were performed on a NM/40 μm glass microballoon mixture, with the concentration of microballoons "volume-matched" to the 6 wt% solid 40 μm bead solutions described above. Figure 8 shows the wave profiles for shot 2S-441, with a shock input pressure of ~ 8.2 GPa. From both the shock wave profiles and run-distance-to-detonation, the hollow microballoons are more sensitizing at the same volumetric loading compared with solid beads of similar diameter. The wave profiles show effective hot spot-driven growth to detonation, Fig. 8, with the increase in particle velocity associated with the build-up to detonation temporally and spatially close to the shock front.

Also, the peak particle velocity at the turnover to detonation remains nearly constant as the wave travels farther into the sample. Once detonating, the profile is marked by a "notch" or sharp inflection near u_p ~ 1.87 mm/μs, similar to the wave structure observed in the small solid bead solutions above (see Fig. 7). The microballoons at this volumetric loading (spaced ~ 106 μm apart) are as sensitizing as the addition of 6 wt% multi-sized rough silica. It is expected that the hollow microballoons collapse under the incident shock, creating hot spots derived from microballoon collapse and jetting at each individual microballoon site.[34]

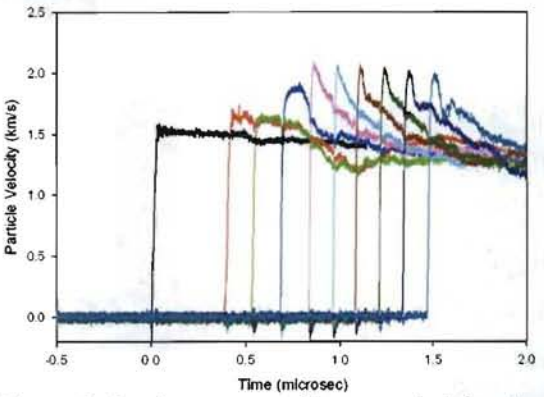

Figure 8. In-situ wave profiles recorded for shot 2S-441, 96.98/1.2/1.84 NM/40 μm balloons/Guar, with an initial shock input pressure of 8.2 GPa.

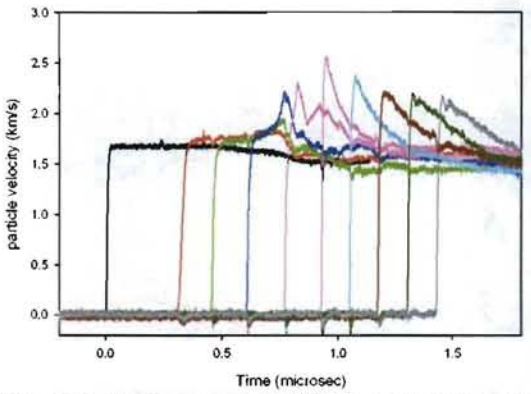

Figure 9. In-situ wave profiles recorded for shot 2S-444, 97.79/0.36/1.85 NM/40 μm balloons/Guar, with an initial shock input pressure of 9.2 GPa.

Decreasing the volumetric concentration of the microballoons, and increasing the inter-balloon spacing to ~158 μm appears to reach a limit of hot spot criticality. Fig. 9 illustrates the effect of increasing the mean inter-hot spot spacing by just over 1 diameter. The shock wave profiles show

evidence, again, of a mixed mechanism, where hot spot-driven burn does not compete effectively with thermal-driven explosion or bulk burn. Furthermore, there appears to be evidence of a secondary reactive build-up behind the superdetonation wave. At the turnover to detonation, the state appears overdriven, consistent with that observed in homogeneous neat NM, and the detonation settles down over measureable time/distance. In contrast to the previous solutions, the detonation profiles appear smooth as the state settles down toward steady detonation.

The Pop-plot data points for the two solutions show the dramatic effect of a small change in hot spot volumetric concentration, Fig. 10. The run-time-to-detonation increases by nearly a microsecond at a similar shock input pressure as the microballoon concentration is decreased, and the hot spots become less effective. The slopes of the respective Pop-plots also change as the initiation mechanism changes. As the build-up to detonation becomes increasingly reminiscent of neat NM, so too, does the slope of the data approach that of neat NM data.

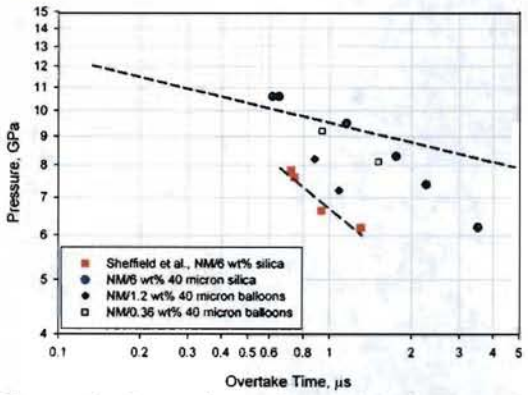

Figure 10. Comparison of Pop-plots for neat NM, NM containing solid silica particles, and NM containing hollow glass microballoons.

Additional experiments employing hollow microballoons as a source of hot spots are necessary to fully understand the critical hot spot features, and compare void collapse to shock impedance mismatches for their respective effectiveness.

Comparison of chemical reaction zones

As mentioned above, the detonation wave profiles appear to be altered in the samples where the initiation behavior is dominated by hot spots. A discontinuity or notch in the detonation profiles is observed near $u_p \sim 1.8$ mm/μs. The notch can be seen clearly in Figs. 7 and 9 for solutions containing the 1-4 μm diameter solid beads and ~ 40 μm diameter microballoons. Based on our recent measurements of the features of the chemical reaction zone according to ZND theory for neat NM,[24] and previous embedded gauge measurements, it is known that the embedded gauge data do not resolve the peak particle velocity due to their inherent temporal response limitations (~10 ns).

We recently reported measurement of the detonation wave profile in neat NM at a NM/PMMA windowed interface, using both VISAR (velocity interferometer for any reflector) and PDV (photon Doppler velocimetry). The experiments measure the detonation wave profile after the wave has propagated ~6 diameters, and it is expected to be steady. For neat NM, the chemical reaction zone has a predicted von Neumann particle velocity of $u_p \sim 2.75$ mm/μs, and sonic locus at ~ 1.8 mm/μs. The decay in particle velocity is smooth, and occurs with both fast (~ 10 ns) and slow (~ 100 ns) components. The measured peak particle velocity in neat NM is lower than expected based on the unreacted and product equations of state, indicating that even the VISAR and PDV diagnostics lack the temporal resolution to resolve the von Neumann spike.

Fig. 11 shows the detonation wave profiles for neat NM and NM containing 1.2 wt% hollow microballoons. There are several key differences between the two profiles, indicating that hot spot-derived burn not only influences the shock-to-detonation transition, but also the nature of energy release in the reaction zone. While the first part of the reaction zone appears similar, there are key differences at later times/distances from the front. The temporal decay occurs over a shorter time period (by ~ 30 ns at $u_p \sim 1.88$ mm/μs) for the microballoon solution. The wave profile for the heterogeneous solution also shows the same notch as observed in the gauge data above, indicating that it is a steady feature.

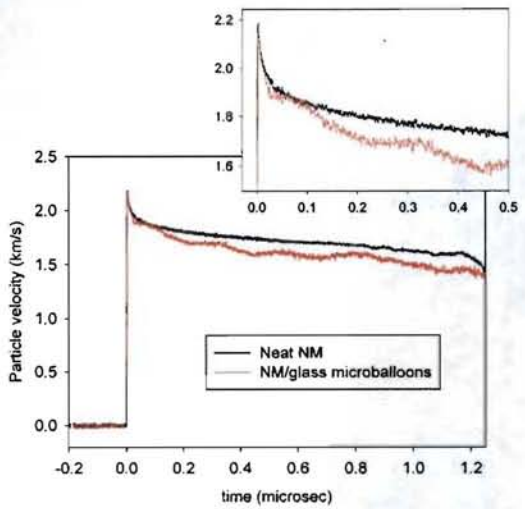

Figure 11. Temporal decay of the chemical reaction zone in neat NM and NM/1.2 wt% 40μ microballoons.

The profile is also distinguished by regular fluctuations in the particle velocity with time (frequency ~ 250 ns, wavelength ~ 4 mm). The fluctuations may be due to transverse wave structures in the heterogeneous solution. Since we do not know the product EOS for NM/microballoon solutions, it is difficult to infer the specific effect(s) of the microballoons on the peak particle velocity and CJ states, but difference in particle velocity could be due to 2-D effects, alteration of the product isentrope due to inert dilution, and/or increased shock temperature associated with the collapse of the microballoons.

Conclusions

The formation and evolution of hot spots are key to the initiation characteristics of heterogeneous high explosives. They have been proposed to arise from many possible sources. Here, we have studied a well-defined, tunable model system to examine two types of potential hot spot origins, as well as gain information on critical hot spot size and spacing (through volumetric concentrations). The reactive flow characteristics, and run distances-to-detonation for gelled NM with 6 wt% silica beads of two discrete sizes have been reported. The smaller beads, which are at a greater number density and closer inter-particle spacings (~ 6 μm), were found to be more sensitizing than the larger beads, which are spaced ~2.5 diameters (106 μm) apart. For the samples containing 6 wt% 40 μm beads, a range of initiation behaviors were observed for the first time. As the initial shock strength was varied, the behavior transitioned from "heterogeneous"-like, with reactive growth near the shock front, at low shock input pressures, to initiation via thermal explosion, and build-up of a reactive wave more characteristic of homogeneous explosives, at high shock pressures. This is one of the few observations of homogeneous initiation behavior in a heterogeneous mixture – e.g. the hot spots are not effective on the time scale of the shock initiation.

Addition of microballoons at nearly the same size and volumetric loading as the 40 μm diameter beads indicates that the collapse of porosity produces more effective hot spots, by increased volumetric hot spot concentration and/or hot spot temperatures. Similar to the NM/bead solutions, we have observed a limit of hot spot criticality in the NM/microballoon solutions. As the inter-balloon spacing is increased from ~ 2.5 to ~ 4 diameters, the initiation behavior becomes dictated by thermal explosion. Clearly, the nature of the shock-to-detonation transition is determined by the complex and competing length and time scales associated with the confluence of hot spots and bulk thermal-driven burn. On-going work is aimed at modeling the formation and evolution of the hot spots derived by the two different shock-driven processes, and their associated temperatures above the bulk shock temperature.

Acknowledgments

Los Alamos National Laboratory is operated by LANS LLC for DOE and NNSA. Funding was provided by LANL Laboratory Directed Research and Development, Project #20080015DR. We gratefully acknowledge project team members for insightful discussions, and the Chamber 9 gas gun team for help with the experiments.

References

1. Bowden, F. P., Yoffe, A. D. *Initiation & growth of explosion in liquids and solids* (Cambridge, 1952).

2. Field, J. E. Acc. Chem. Res. 25, 489-496 (1992).
3. Bourne, N. K.; Field, J. E. *Proc.: Math., Phys., Eng. Sci.*, **455**, 2411 (1999).
4. Engelke, R. *Phys. Fluids*, **22**(9), 1623 (1979).
5. Engelke, R. *Phys. Fluids*, **26**(9), 2420 (1983).
6. Sheffield, S. A.; Dattelbaum, D. M. et al. in 13th International Sympsium on Detonation, Office of Naval Research, ONR 351-07-01, 401 (2006).
7. Ramsay, J. B.; Popolato, A. Fourth Symposium (International) on Detonation, Office of Naval Research Report # ACR-126, p 233 (1965).
8. Chick, M. C. Fourth Symposium (International) on Detonation, Office of Naval Research, ACR-126, 349-358 (1965).
9. Price, D. Fifth Symposium (International) on Detonation, Office of Naval Research, ACR-184, 207-217(1970).
10. Scott, C. L. Fifth Symposium (International) on Detonation, Office of Naval Research, ACR-184, 259-266 (1970).
11. Seely, L. B. Proceedings of the Fourth Elecric Initiator Symposium, Franklin Institute, PA, Paper 27 (1963).
12. Simpson, R. L.; Helm, F. H. et al. Ninth Symposium (International) on Detonation, OCNR-113291-7, 25-38 (1989).
13. Setchell, R. E. Eighth Symposium (International) on Detonation, NSWC MP 86-194, 15-25 (1985).
14. Moulard, H. Ninth Symposium (International) on Detonation, OCNR-113291-7, 18-24 (1989).
15. Moulard, H.; Kury, J. W.; Delclos, A. Eighth Symposium (International) on Detonation, NSWC MP 86-194, 902-913 (1985).
16. Lee, E. L.; Tarver, C. M. Phys. Fluids, 23, 2362-72 (1980).
17. Presles, H.-N. *et al.* Shock Waves, 4, 325-329 (1995).
18. Khasainov, B. A.; Ermolaev, B. S.; Presles, H.-N.; Vidal, P. Shock Waves, 7, 89-105 (1997).
19. Bouton, E. *et al.* Shock Waves, 9, 141-147 (1999).
20. Howe, P.; Frey, R.; Taylor, B.; Boyle, V. Sixth Symposium (International) on Detonation, Office of Naval Research, ACR-221, 11-19 (1976).
21. Sheffield, S. A.; Alcon, R. R. *Shock Compression of Condensed Matter-1989*, 683 (1990).
22. Gustavsen, R. L.; Sheffield, S. A.; Alcon, R. R. "*High Pressure Science and Technology - 1993, Pts 1 and 2,* 1703-1706 (1994).
23. Alcon, R. R.; Sheffield, S. A.; Martinez, A. R.; Gustavsen, R. L.; *AIP Conference Proceedings* **429**, 845 (1998).
24. Bouyer, V.; Sheffield, S. A.; Dattelbaum, D. M.; Gustavsen, R. L.; Stahl, D. B.; Doucet, M.; Decaris, L. *AIP Conference Proceedings*, **1195**, 175 (2009).
25. Engelke, R. *Phys. Fluids*, **23**(5), 875 (1980).
26. Campbell, A. W.; Davis, W. C.; Travis, J. R. *Phys. Fluids*, **4**, 511 (1961).
27. Chaiken, R. F. *J. Chem. Phys.*, **33**, 760 (1960).
28. Sheffield, S. A.; Engelke, R.; Alcon, R. R. in Ninth Symposium (International) on Detonation; 1989.
29. Hardesty, D.R.; Lysne, P. C. "Shock initiation and detonation properties of homogeneous explosives" Sandia Report no. SLA-74-165, 1974-05-01.
30. Voskoboinikov, I. M.; Bogomolov, V. M.; Apin, A. Ya. *Fizika Goreniya I Vzryva*, **4**, 45-49 (1968).
31. Leal, B. *et al.* In Proceedings of the 11th Symposium (International) on Detonation.
32. Engelke, R.; Sheffield, S. A.; Stacy, H. L. Phys. Fluids, 16, 4143 (2004).
33. Engelke, R.; Sheffield, S. A.; Stacy, H. L. Phys. Fluids, 17, 096102 (2005).
34. Menikoff, R. personal communication, Los Alamos National Laboratory, November 2009.
35. Gustavsen, R. L.; Sheffield, S. A.; Alcon, R. R.; Hill, L. G.; "Shock Initiation of New and Aged PBX 9501 Measured with Embedded Electromagnetic Particle Velocity Gauges," Los Alamos National Laboratory Report, LA-13634-MS.
36. Dattelbaum, D. M.; Sheffield, S. A.; Stahl, D. B.; Dattelbaum, A. M. *AIP Conference Proceedings*, **1195**, 261 (2009).